

Surface effects in nanoparticles

H. Kachkachi*, A. Ezzir, M. Noguès,
*LMOV-CNRS UMR 8634,
Université de Versailles St. Quentin,
45, avenue des Etats-Unis,
78035 Versailles Cedex, France*

E. Tronc
*LCMC-CNRS URA 1466,
Université Pierre & Marie Curie,
4 place Jussieu, 75252 Paris Cedex, France.*

We present a microscopic model for nanoparticles and perform Monte Carlo simulations of their magnetic properties. On account of Mössbauer spectroscopy and high-field magnetization results, we consider a particle as containing a magnetically ordered core and a relatively disordered surface. The magnetic state in the particle is described by the anisotropic classical Dirac-Heisenberg model including exchange and dipolar interactions and bulk and surface anisotropy. We consider the case of ellipsoidal (or spherical) particles with free boundaries at the surface. Using a surface shell of constant thickness (~ 0.35 nm) we vary the particle size and study the effects of surface disorder on the thermal and spatial behaviors of the net magnetization of the particle. We study the shift in the surface “critical region” for different surface-to-core ratios of the exchange coupling constants. It is also shown that the profile of the local magnetization exhibits strong temperature dependence.
PACS : **75.30.Pd** (surface magnetism), **75.50.Gg** (ferrimagnetism), **75.60.Jp** (nanoparticles).

I. INTRODUCTION

Surface effects in a nanoparticle are of great importance since they dominate the magnetic properties and become more important with decreasing size of the particle. In particular, the picture of a single-domain magnetic particle where all spins are pointing into the same direction, leading to coherent relaxation processes, is no longer valid when one considers the effect of disordered spins on the surface on the global magnetic properties of the particle. Indeed, even for strong exchange interactions the surface is responsible for coordination defects, and in a particle of radius of the order of 4 nm, 50% (in the γ - Fe_2O_3 nanoparticles) of atoms lie on the surface, and therefore the effect of the latter can not be neglected.

The magnetization near the surface is generally lower than in the interior. This effect leads to a thermodynamic perturbation in exchange interactions near the surface, which can be sizable at high temperatures. In a finite system, the effect of temperature introduces, in addition to the usual renormalization of the spin-wave spectrum, a spatial dependence of the magnetization (see [1] and references therein for the case of semi-infinite cubic crystals). Indeed, the symmetry breaking at the surface results in a surface anisotropy. In most cases, this happens to be strong enough as to compensate for the work needed against the exchange energy that prefers full alignment, and it is conceivable then that the magnetization vector will point along the bulk easy axis in the core of the particle, and will then gradually turn into a different direction when it approaches the surface. In addition to the exchange interactions, which are the strongest interactions between atoms in a magnetic system, there are also the purely magnetic dipole interactions between the magnetic moments of the atoms and the interactions between the magnetic moments and the electric field of the crystal lattice (spin-orbit interactions). The last two types of interactions are relativistic in origin and therefore correspond to energies that are much smaller than the exchange energy on a short length scale, but as they are long range interactions they lead, in general, to non negligible contributions. Indeed, these interactions play an important role in that they introduce a preferred direction in the system as they correspond to a Hamiltonian (see below) that is not invariant under rotation operations. In other words, they lead to the appearance of an anisotropy energy, i.e. the dependence of the total energy of the system on the direction of magnetization. Moreover, the most important feature of the relativistic interactions is that they change the magnetic moment of an atom from one site to another, and hence introduce a non uniform spatial distribution of the magnetic moment in the system. The treatment of the dipole-dipole interactions [2] leads to two energy terms corresponding to the volume and surface charges. In a small

*Corresponding author : kachkach@physique.uvsq.fr

magnetic system, such as a nanoparticle, only the second contribution is important since it accounts for the shape anisotropy, and the former becomes negligible as one integrates over a small volume (see a detailed discussion in [3] and references therein).

To sum up, it is necessary to take into account all different contributions to the energy, exchange and dipolar interactions, bulk and surface anisotropies, in any study of spatial distributions of the magnetization in a small magnetic system.

Therefore, we need to understand the surface effects on the thermodynamic and spatial behaviors of the magnetization in small systems, since this is also of crucial importance to the study of the dynamics of such systems where the surface effects are considerable. In this case the dynamics is rendered more complicated by the additional (metastable or stable) magnetic states corresponding to the surface configurations.

According to Mössbauer spectroscopy performed by Morrish et al. (see the review [4], and also the seminal work by Coey [5]), the iron cations at the surface of the $\gamma\text{-Fe}_2\text{O}_3$ particles have a noncollinear magnetic structure from 4.2 K to room temperature.

The Mössbauer-spectroscopy analysis performed in [6] on $\gamma\text{-Fe}_2\text{O}_3$ particles show that the spectrum contains two components, one associated with the bulk and the other with iron atoms on the surface. The latter seems to disappear at temperatures in the range 75 – 100 K, depending on the mean diameter of the particle assembly. From these Mössbauer-effect analyses it was also inferred that the surface shell has a thickness of about 0.35 nm, independently of the particle volume. This fact will be used in our simulations to determine the ratio of the surface and core number of atoms.

In addition, measurements of the magnetization at high fields performed on the $\gamma\text{-Fe}_2\text{O}_3$ nanoparticles [7] (see also [8] for cobalt particles) have shown that the magnetization is strongly influenced by the surface effects, depending on the particle size. In Figs.1 we show the field and thermal variation of the magnetization for different particle sizes. In Fig.1a we see that there is a sudden increase of the magnetization as a function of the applied field when the temperature reaches 70 K, and that the magnetization does not saturate at the highest field value, i.e. 5.5 T. In Fig.1b there is an important increase of the magnetization at low temperatures. In Fig.1c the thermal behaviour of the magnetization at 5.5 T is shown for samples with different mean diameter. There we see that the smaller is the mean diameter of the particle the more important is the increase of the magnetization at very low temperatures. This can be explained by the fact that the surface component corresponds to a state with canted atomic moments at low temperatures [5] [6].

Furthermore, open hystereses were observed [9] in the nickel ferrite particles (NiFe_2O_4) up to fields of 16 T, while the anisotropy field of the bulk sample is utmost 4×10^{-2} T. The authors consider that the core spins are colinear whereas those on the surface are disordered. In the case of $\gamma\text{-Fe}_2\text{O}_3$ particles, however, no such irreversibility in the magnetization hysteresis loop was observed [6], [9].

Therefore, according to Mössbauer spectroscopy and high-field magnetization measurements, we may think of a particle as containing a disordered surface of a certain width and a core more or less ordered depending on the size of the particle. The net magnetization of the particle is given by the sum of the contributions from the surface and the core. The increase of surface contribution at low temperatures becomes more important with decreasing size of the particle, as shown in Fig.1c.

In this work, we compute the thermal behavior of the different contributions to the magnetization due to the surface and core for different values of exchange couplings and different surface to volume ratios. We also compute the spatial variation of the magnetization at different temperatures and the specific heat for different sizes. All calculations are performed in zero magnetic field, the field effect will be studied in a subsequent work.

II. MODEL FOR MAGNETIC PARTICLES

A. Hamiltonian

As was discussed in the introduction, it is well established [2], [3] that any theory dealing with the spatial magnetization distribution must consider all three energy contributions, exchange, anisotropy and magnetostatic, and that there is no obvious reason for neglecting any one of these. However, it should be emphasized that in small particles the exchange interactions are too strong to allow for subdivision into domains, so that the magnetostatic energy term is considered here only in order to account for the shape anisotropy in the case of ellipsoidal particles. It should also be stressed, as discussed in the introduction, that because of the surface anisotropy and the symmetry breaking at the surface, there is no reason to consider the exchange interactions on the surface as equal to those in the core, and thereby the particle may acquire a non uniform distribution of the magnetization.

Therefore, to take account of all these energy contributions, we propose a model, based on the classical Dirac-Heisenberg (exchange and dipolar) Hamiltonian, describing the spinel structure of the (spherical or ellipsoidal) ferrimagnetic nanoparticles (e.g., γ -Fe₂O₃). In this article the calculations are performed using Monte Carlo simulations of the magnetization thermal behavior of the particle with open boundaries at the surface.

So, the exchange, anisotropy and Zeeman contributions are given by the following anisotropic Dirac-Heisenberg Hamiltonian

$$\mathcal{H}_{DH} = - \sum_{i,\mathbf{n}} \sum_{\alpha,\beta=A,B} J_{\alpha\beta} \mathbf{S}_i^\alpha \cdot \mathbf{S}_{i+\mathbf{n}}^\beta - K \sum_{i=1}^{N_t} (\mathbf{S}_i \cdot \mathbf{e}_i)^2 - (g\mu_B)H \sum_{i=1}^{N_t} \mathbf{S}_i$$

where $J_{\alpha\beta}$ (positive or negative) are the exchange coupling constants between (the $\alpha, \beta = A, B$) nearest neighbors spanned by the unit vector \mathbf{n} ; \mathbf{S}_i^α is the (classical) spin vector of the α^{th} atom at site i ; H is the uniform field applied to all spins (of number N_t) in the particle, $K > 0$ is the anisotropy constant and \mathbf{e}_i the single-site anisotropy axis (see below). A discussion of the core and surface anisotropy will be presented below. In the sequel the magnetic field will be set to zero.

To the Dirac-Heisenberg Hamiltonian we add the pairwise long-range dipolar interactions

$$\mathcal{H}_{dip} = \frac{(g\mu_B)^2}{2} \sum_{i \neq j} \frac{(\mathbf{S}_i \cdot \mathbf{S}_j) R_{ij}^2 - 3(\mathbf{S}_i \cdot \mathbf{R}_{ij}) \cdot (\mathbf{R}_{ij} \cdot \mathbf{S}_j)}{R_{ij}^5}$$

where g is the Landé factor, μ_B the Bohr magneton and \mathbf{R}_{ij} the vector connecting any two spins on sites i and j inside the particle, $R_{ij} \equiv \|\mathbf{R}_{ij}\|$.

B. Method of simulation

The particle we consider here is a spinel with two different iron sites, a tetrahedric Fe³⁺ site (denoted by A) and an octahedric Fe³⁺ site (denoted by B). The nearest neighbor exchange interactions are (in units of K) [10], [9] : $J_{AB}/k_B \simeq -28.1$, $J_{BB}/k_B \simeq -8.6$, and $J_{AA}/k_B \simeq -21.0$. These coupling constants are used in the Dirac-Heisenberg Hamiltonian \mathcal{H}_{DH} in order to model the phase transition from the paramagnetic to ferrimagnetic order as the temperature is lowered down to zero through $T_c \simeq 906$ K. In the spinel structure an atom on site A has 12 nearest neighbors on the sublattice B and 4 on the sublattice A, and an atom on site B has 6 nearest neighbors on A and 6 on the B sublattice; the number of B sites is twice that of sites A. The nominal value of the spin on sites A and B is 5/2.

We have also taken account of $\frac{1}{3}$ of lacuna for each two B atoms randomly distributed in the particle.

The nanoparticle we have studied contains N_t spins ($\simeq 10^3 - 10^5$), and its radius (denoted by R_t) is in the range 2-3.5 nm. Our model is based on the hypothesis that the particle is composed of a core of radius $R_c \leq R_t$ containing N_c spins, and a surface shell surrounding it that contains N_s spins, so that $N_t = N_c + N_s$. Thus varying the size of the particle while maintaining the thickness of the surface shell constant (~ 0.35 nm), is equivalent to varying the surface to total number of spins, $N_{st} = N_s/N_t$, and this allows us to study the effect of surfaces of different contributions. All spins in the core and on the surface are identical, but interact via the, *a priori*, different couplings depending on their locus in the whole volume. We will consider both cases of identical interactions, and that of the general situation with different interactions on the surface and core. Although we treat only the crystallographically “ideal” surface, we do allow for perturbations in the exchange constants on the surface. This is meant to take into account, though in a somewhat phenomenological way, the possible defects on the surface, and the possible interactions between the particles and the matrix in which they are embedded. In [9] it was assumed that the pairwise exchange interactions are of the same magnitude for the core and surface atoms, but there was postulated the existence of a fraction of missing bonds on the surface.

On the other hand, we consider that the exchange interactions between the core and surface spins are the same as those inside the core. We also stress that we are only concerned with non interacting particles, so we ignore the effect of interparticle interactions on the exchange couplings at the surface of the particle.

We start with a regular box ($X \times Y \times Z$) of spins with the spinel structure having the properties mentioned above, and then given the radius R_t or total number of spins in the particle, we cut in a sphere or an ellipsoid. We choose the center of the particle to lie at one of the lattice sites. Thus, a spin of spatial coordinates (x, y, z) contained in a sphere of total radius R_t is defined as a core spin if $\sqrt{x^2 + y^2 + z^2} \leq R_c$, or as a surface spin if $R_c < \sqrt{x^2 + y^2 + z^2} \leq R_t$, and similarly for a spin in an ellipsoidal particle. In all cases free boundary conditions are used, and the sites on the boundary of the particle thus have automatically less neighbors to which they are exchange coupled, than those in the

core whose coordination numbers correspond to the bulk material. Fig.2 shows the distribution of the coordination numbers in a spherical and ellipsoidal particle.

Therefore, in our simulations each spin has a structure associated with it that contains the coordinates of the corresponding site, the nature of the site in the spinel structure (i.e. A or B), its locus (core or surface), the number of its nearest neighbors, and the total number of such sites. Thus, once the structure of each spin is defined, the spins outside of the sphere or the ellipsoid are discarded.

Anisotropy energies : In both cases of a spherical and ellipsoidal particle, we consider a uniaxial anisotropy in the core and single-site anisotropy on the surface. The easy axis in the core is chosen along our z reference axis, and the sites on the boundary have uniaxial anisotropy, with equal anisotropy constant K_s , whose axes \mathbf{e}_i are chosen to point outward and normal to the surface ([9], [12]). More precisely, we define for each spin a unit gradient vector on which the spin magnetic moment has to be projected. In the case of a spherical particle these anisotropy axes are along the radius joining the center of the particle to the considered surface site.

For an ellipsoidal particle the easy direction in the core is taken along the major axis of the ellipsoid, which is also along the z direction. The bulk anisotropy constant was estimated by many authors (see e.g. [11] and references therein) to be $K_1 \simeq 4.7 \times 10^4$ erg/cm³. In our simulations we normalized this constant to the number of sites and in units of K , $k_c \equiv (K_c/k_B) \simeq 8.13 \times 10^{-3}K$, k_B being the Boltzmann constant. On the other hand, the surface anisotropy has not been determined experimentally in magnetic oxides, but it has become clear, however, that the corresponding contribution is very large as compared with the bulk one. In our calculations we took $k_s \equiv (K_s/k_B) \simeq 0.5$ K; the corresponding surface anisotropy constant K_s was estimated to be $\simeq 0.06$ erg/cm² (see [13], [14]). In [9] k_s was taken in the range 1 – 4 K, but for these higher values of surface anisotropy the authors obtained high-field irreversibility whereas the experimental results (also presented in [9]) show none for the γ -Fe₂O₃ particles.

Finally, in the case of an ellipsoidal particle, as discussed at the beginning of sect.2.A, the effect of the dipolar interactions \mathcal{H}_{dip} boils down to a mere shape anisotropy, which is absent in a spherical particle. Therefore, the magnetostatic energy of an ellipsoid of semi-axes $\frac{X}{2}, \frac{Y}{2}, \frac{Z}{2}$, can be written as [2], [3]

$$E_{mag} = \frac{1}{2V} (D_x \cdot M_x^2 + D_y \cdot M_y^2 + D_z \cdot M_z^2)$$

where $D_\alpha, \alpha = x, y, z$, are the demagnetizing factors, $M_\alpha, \alpha = x, y, z$, the components of the net magnetization, and V the volume of the particle, which is equal to N_t in our calculations. If all semi-axes are different it is not possible to express the D 's in closed form. However, this is possible in the case of a prolate or oblate spheroid. In the case of a prolate spheroid, as is very common in permanent magnet materials, i.e. $Z > X = Y$, the demagnetizing factors are given by [15]

$$D_z = 4\pi \frac{1-e^2}{2e^3} \left[\log \left(\frac{1+e}{1-e} \right) - 2e \right],$$

$$D_x = D_y = \frac{1}{2}(4\pi - D_z),$$

where $e = \sqrt{1 - (X/Z)^2}$, $0 < e < 1$, is the eccentricity of the ellipsoid. In these calculations we assumed that the easy axes of the magnetocrystalline and shape anisotropy are the same, though this is not the case in general.

We have found that using the long-range dipolar interactions \mathcal{H}_{dip} , involving all possible pairs of atoms in the particle, or the macroscopic magnetostatic energy E_{mag} yields within numerical errors, the same results, only that the former contribution is much more time consuming than the latter.

C. Results and discussion

1. Thermal variation of the magnetization

In Figs.3a-c, we plot the computed thermal variation of the core and surface contributions to the magnetization (per site) as a function of the reduced temperature $\tau^{core} \equiv T/T_c^{core}$. There the number of spins $N_t = 909, 2009, 3766$ and the surface contribution $N_{st} = 53\%, 46\%, 41\%$, respectively. These values of N_{st} have been determined by the fact that the thickness of the surface shell is constant (~ 0.35 nm), according to Mössbauer-effect analysis. They correspond to a diameter of circa 4, 4.6 and 6 nm, respectively.

In Fig.3d we plot the mean magnetization defined as $M_{mean} \equiv \frac{N_s M_{surf} + N_c M_{core}}{N_t}$ as a function of the reduced temperature $\tau^{core} = T/T_c^{core}$, T_c^{core} being here the highest core critical temperature, for the same values of N_{st} as

above. The exchange coupling in the core (i.e. J_{AA}, J_{AB}, J_{BB}), generically denoted by J_c , are taken as 10 times those on the surface, denoted by J_s . Since there is no experimental estimation of the exchange couplings on the surface, the choice of such J_s was guided by the fact that the critical temperature of the bulk material is circa 906 K, while the hypothetical surface transition occurs in the temperature range of 75 – 100 K (which is a factor of 9 to 10 smaller) according to Mössbauer spectroscopy and high-field magnetization measurements. Nevertheless, we have also considered the effect of other ratios J_c/J_s (see below).

We see that the surface “critical region”, corresponding to the magnetic phase transition on the surface is in a range of temperatures lower than the critical temperature of the core. This is expected from the fact that since the molecular field acting on a surface spin is lower than the one acting on a core spin, as a consequence of the lower coordination number at the surface and hence the change in crystal field thereon [1], [16], and also because of the fact that J_s are taken to be smaller than J_c . This is in agreement with the results of Mössbauer spectroscopy and the magnetization measurements at high fields, since the surface component has a “critical temperature” in the range 75 – 100 K while for the core component the critical temperature is much higher ($\simeq 906$ K).

Note that both transitions are smeared because of the finiteness of the system size.

We also note that the surface magnetization $M_{surface}$ decreases more rapidly than the core contribution M_{core} as the temperature increases, and has a positive curvature while that of M_{core} is negative, as is most often the case. Moreover, it is seen that even the (normalized) core magnetization per site does not reach its saturation value of 1 at very low temperatures, and this can be explained by the fact that the magnetic order in the core is disturbed by the relative disorder on the surface, or in other words, the magnetic disorder starts at the surface and gradually propagates into the core of the particle (see Fig.6 below). In Fig.3d we see that the more important is the surface contribution the more enhanced and rapid is the raising of the mean magnetization at low temperatures, and this behaviour bears some resemblance to Fig.1c.

In Fig.4 we plot the core ($N_t = 909, 3766, 6330$) and bulk¹ magnetization as a function of the reduced temperature $\tau^{bulk} \equiv T/T_c^{bulk}$, the corresponding values of N_{st} being 53%, 41%, 26%, respectively. Comparing the different curves, it is seen that both the critical temperature T_c and the value of the magnetization are dramatically reduced in the core of the particle. The reduction of T_c is obviously due to the finite-size and surface effects. There is a size-dependent reduction of the critical temperature by up to 50% for the smallest particle. The same result has been found by Hendriksen et al. [17] for small clusters of various structures (bcc, fcc, and disordered) using spin-wave theory. As to the magnetization, the reduction shows that the core of the particle does not possess the same magnetic properties as the bulk material, but as said before, it is influenced by the relatively disordered surface.

In Fig.4 we can also see that T_c increases with the particle size N_t , since the higher is the latter the lower is the magnetization in the critical region and the higher is the temperature at which the magnetization approaches zero. However, the increase of T_c with N_t is not as clear-cut as it could be expected, and this can be understood by noting that the disordered surface ($J_s = J_c/10$, and small coordination numbers) strongly influences the magnetic order in the core through the relatively strong exchange couplings between surface and core spins, which are equal to those in the core.

2. Effect of the ratio J_c/J_s

In Fig.5 we plot the thermal variation of the surface contribution to magnetization as a function of the reduced temperature τ^{core} for the case of $J_s = J_c/2, J_c$ and $2J_c$, and for $N_t = 5269$ and $N_{st} = 40\%$. Here the thickness of the surface shell is greater than 0.35 nm, and is not taken from experiments, contrary to the values in Figs.3. The reason for taking such N_{st} is merely to compare the results for surfaces with different thickness. At any rate, our aim here is to maintain N_{st} fixed to a given value and vary the ratio J_c/J_s .

We see that the surface critical region is shifted to higher temperatures upon increasing J_s , and only when $J_s = 2J_c$ that both the core and surface magnetic phase transitions occur in the same temperature range, i.e. $\tau^{core} \simeq 1$. It is worth noting that the weaker is the exchange interactions on the surface the lower is the magnetization of the latter.

This result remains the same upon lowering the surface width. In this case the number of spins having smaller coordination numbers, and hence weaker effective exchange energy, i.e. those spins on the outer shell of the particle, is very small as compared with the rest of spins in the particle. Moreover, we may think that the spins on the outer

¹The bulk here refers to the perfectly ferrimagnetic material with periodic spinel structure and without vacancies, though such material does not exist in reality since all spinels present some degree of vacancy.

shell follow the (strong) molecular field created by the other (inner) spins constituting a ferrimagnetically ordered core.

Setting $J_c = \lambda J_s$, we may determine the coefficient λ at which the transition regions of the core and surface overlap. This may be done using the simple, though time consuming, cumulant method introduced a few years ago by Binder (see [18] for a review). This will be done in a subsequent work [19].

3. Profile of the magnetization

We have determined the spatial variation of the mean magnetization of a spherical particle as we move from the center out onto the surface, for different temperatures. At nearly zero temperature (Fig.6a), the mean magnetization decreases with increasing particle radius. It starts from the saturation value of an iron atom (in fact, we computed the mean value of A and B atoms, to take into account the possibility of starting at either atom) at the center of the particle and decreases down to the value of a surface atom. Note that what is plotted in Figs.6 is in fact the (normalized) projection of the atomic magnetic moment along the easy axis (z-axis for the core, and normal for the surface spins), which is proportional to $\cos \theta$, and thus Figs.6 also show the spatial evolution of the orientation of the magnetic moment inside the particle.

The decreasing of the local magnetization shows that even at very low temperature the surface is in a magnetic order which is different from that in the core and as discussed earlier, the magnetic disorder starts at the surface and gradually propagates into the core. This could be related with the gradual canting of spins confirmed by Mössbauer spectroscopy [5], [6]. As the temperature increases (Fig.6b), the local magnetization exhibits a jump of temperature-dependent height at nearly the same position on the radius vector, and continues to decrease.

Since the local magnetization depends on the direction of the radius vector, especially in an ellipsoidal particle, the curves in Fig.6b present, in addition to the usual numerical inaccuracy, some fluctuations due to the spatial non homogeneities inherent to the lacunous spinel structure of the $\gamma\text{-Fe}_2\text{O}_3$ particles ($\frac{1}{3}$ for each two B atoms randomly distributed).

4. Specific heat

In Fig.7 we plot the computed specific heat for the bulk with boundary conditions, $N_t = 909, 3766, 6330$ and the corresponding values of N_{st} given above. There is a phase transition marked by a well defined peak for the bulk and a broad peak for the three particle sizes. This broadening is an obvious illustration of the finite-size effects. Note also the shift by 50% to lower temperatures of the critical region, as in the magnetization thermal behaviour in Fig.4.

It should be very interesting to have adequate samples for specific heat measurements. To our knowledge, such measurements have never been performed on nanoparticle assemblies.

III. CONCLUSION

We have presented a microscopic model for magnetic nanoparticles including exchange and dipolar interactions, and bulk and surface anisotropy, and investigated the thermal and spatial behaviours of the core and surface contributions to the net magnetization of a nanoparticle of different sizes, and hence of different surface contributions. We have found that the finiteness of the system size and free boundaries lead to a non uniform magnetization profile decreasing toward the surface in the particle. This result is in agreement with the spin-wave calculations for small clusters performed in [17].

In order to compare these results obtained for a single nanoparticle with our experiments on dilute assemblies of nanoparticles [7], and in particular to compare with the curve of magnetization vs. temperature given in Fig.1b, we have to include the Zeeman energy term in our Hamiltonian and run our program for different particle sizes with randomly distributed easy axes. This work is now in progress.

From the present single-particle study we can infer some conclusions about the effect of surface disorder on the global magnetic properties of nanoparticles. The surface contribution to the magnetization presents a rather different behaviour from the core contribution. Furthermore, even at very low temperature, the local magnetization decreases with the distance from the center, showing that the magnetic state on the surface is certainly different from that in the core, but this state still has to be understood and compared with the canted state observed in Mössbauer effect measurements. In fact, we still need to understand if there is or not some regular structure in the surface magnetic state. We have also shown that there is a drastic reduction of both the critical temperature and the value of the

magnetization in the core of the particle. The reduction of the former is obviously due to the finite-size and surface effects. As to the magnetization, the reduction shows that the magnetic properties of the particle core are different from those of bulk material, because of the strong influence of the surface magnetic disorder which propagates from the boundary into the core.

We note that our results on the thermal and spatial behaviour of the magnetization are in qualitative agreement with those obtained by Wildpaner [20] for spherical particles with simple-cubic crystalline structure.

In the forthcoming work [19], we take into the account the effect of a magnetic field on the results presented here, and in particular, we study the surface effects on the hysteresis loops of the γ -Fe₂O₃ particles. In Refs. [12] the authors studied the influence of the surface on hysteresis loops in a spherical particle with simple cubic structure using the Landau-Lifchitz-Gilbert equations at zero temperature. The main feature of the loops calculated concerns the steps in the magnetization with linear rising between steps. The appearance of these steps was interpreted as the fact that the core reverses more or less as a unit, while the surface spins reverse in smaller groups. In addition, it was found that the hysteresis loop becomes narrower for higher values of the surface anisotropy.

No such steps were observed [9] in the hysteresis loops of the γ -Fe₂O₃ nanoparticles, and this probably is due to the rounding-off effect induced by the volume distribution. So it should be interesting to investigate this effect in such particles [19] including thermal fluctuations.

Acknowledgments

HK thanks D. Garanin for his valuable remarks and suggestions. The present numerical calculations have been performed on the Alpha Work Station of the Genome Laboratory of the University of Versailles to which we are greatly indebted.

- [1] R. E. De Wames and T. Wolfram, *Progress in Surface Sciences* **2**, ed. by S.G. Davison, Oxford Pergamon, 1972, p.23; T. Kaneyoshi, *J. Phys. Cond. Mat.* **3** (1991) 4497-4522; D. Garanin, *J. Phys. A: Math. Gen.* **29** (1996) L257-L262; D. Garanin, “*Semi-infinite anisotropic spherical model: Correlations at $T \geq T_c$* ”, submitted to *Phys. Rev. E*, January 1998.
- [2] A.I. Akhiezer, V.G. Bar'yakhtar and S.V. Peletinskii, *Spin waves*, North-Holland Publ. Company, 1968.
- [3] A. Aharoni, *Introduction to the theory of ferromagnetism*, Oxford Science Pubs., 1996.
- [4] K. Haneda, *Can. J. Phys.* **65** (1987) 1233, and references therein.
- [5] J.M.D. Coey, *Phys. Rev. Lett.* **27** (1971) 1140.
- [6] P. Prené et al., *Hyperfine Int.* **93** (1994) 1049; P. Prené, Ph.D. thesis of the Université Pierre & Marie Curie, July 1995; E. Tronc et al., *Hyp. Int.* **112** (1998) 97.
- [7] A. Ezzir, Ph.D. thesis of the Université de Paris XI-Orsay, December 1998.
- [8] J.P. Chen et al., *Phys. Rev. B* **51** (1995) 11527.
- [9] R. H. Kodama, A. E. Berkovitz, E.J. Mcniff, and S. Foner, *Phys. Rev. Lett.* **77** (1996) 394; R. H. Kodama and A. E. Berkovitz, “*Atomic-Scale Magnetic Modeling of Oxide Nanoparticles*”, preprint 1998; and references therein.
- [10] J. S. Smart, in *Magnetism*, eds. G.T. Rado and H. Suhl, Academic Press New York 1963, p.63.
- [11] S. Krupicka and K. Zaveta, in *Magnetic Oxides*, Part I, ed. D.J. Craik, A Wiley-Interscience Publication, 1975.
- [12] D. A. Dimitrov and G. M. Wysin, *Phys. Rev. B* **50** (1994) 3077; *ibid* **51** (1994) 11947.
- [13] J.L. Dormann et al., *Phys. Rev. B* **18** (1996) 1; F. Gazeau et al., *Europhys. Lett.* **40** (1997) 575.
- [14] A. Aharoni, *J. Appl. Phys.* **81** (1997) 830.
- [15] B.K.P. Scaife, *Principles of dielectrics*, Oxford Science Pubs., 1989.
- [16] O. Eriksson et al., *Phys. Rev. B* **45** (1992) 2868-2875.
- [17] P.V. Hendriksen, S. Linderoth, and P.-A. Lindgard, *Phys. Rev. B* **48** (1993) 7259.
- [18] K. Binder and D.W. Heermann, “*Monte Carlo simulation in statistical physics*”, Springer-Verlag, Berlin 1992; K. Binder, *Physica* **62** (1972) 508-526; K. Binder and D. Landau, *Surface Science* **151** (1985) 409-429.
- [19] H. Kachkachi, in preparation.
- [20] V. Wildpaner, *Z. Physik* **270** (1974) 215-223.

Figure Captions

Figure 1 :

- a) Magnetization as a function of the magnetic field of a diluted assembly of $\gamma\text{-Fe}_2\text{O}_3$ nanoparticles with a mean diameter of 2.7 nm.
- b) Thermal variation of the magnetization extracted from a) at a field of 55 kOe.
- c) Thermal variation of the magnetization in a field of 55 kOe for three samples with different mean diameters (2.7, 4.8, 7.1 nm).

Figure 2 : Normalized distribution of the coordination number in a spherical and ellipsoidal particle for $N_{st} = 40\%$.

Figure 3 : Thermal variation of the surface and core contributions (Figs.3a-c) to the net magnetization and mean magnetization (Fig.3d) as obtained from the Monte Carlo simulations of an ellipsoidal nanoparticle. The anisotropy constants are given in the text; the exchange interactions on the surface are taken to be 1/10 times those in the core.

Figure 4 : Thermal variation of the bulk and core magnetization as a function of τ^{bulk} (see text), for $N_t = 909, 3766, 6330$ with $N_{st} = 53\%, 41\%, 26\%$, respectively. The exchange interactions on the surface are taken equal to 1/10 times those in the core .

Figure 5 : The computed thermal variation of the surface contribution to the net magnetization of an ellipsoidal nanoparticle as a function of the reduced temperature τ^{core} for $J_s = J_c/2, J_c, 2J_c$ (see text).

Figure 6 : a) Spatial variation of the net magnetization of a spherical nanoparticle of 3140 spins, as a function of the normalized particle radius, for a) $\tau^{core} \ll 1$, and b) $\tau^{core} \ll 1, \tau_c = 0.5$, and $\tau_c \lesssim 1$.

Figure 7 : Thermal behaviour of the specific heat as a function of τ^{bulk} for $N_t = 909, 3766, 6330$ and bulk, and for the same energy parameters as in Figs.3.

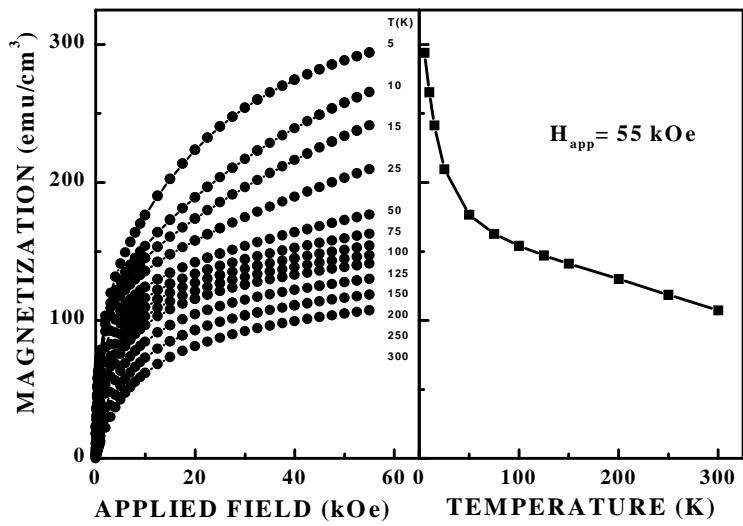


Fig. 1a

Fig. 1b

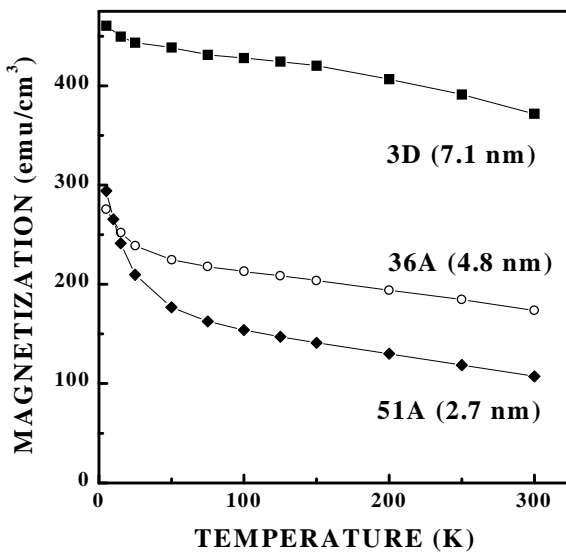


Fig. 1c

This figure "fig2.JPG" is available in "JPG" format from:

<http://arxiv.org/ps/cond-mat/9903398v3>

This figure "Fig3a.JPG" is available in "JPG" format from:

<http://arxiv.org/ps/cond-mat/9903398v3>

This figure "Fig3b.JPG" is available in "JPG" format from:

<http://arxiv.org/ps/cond-mat/9903398v3>

This figure "Fig3c.JPG" is available in "JPG" format from:

<http://arxiv.org/ps/cond-mat/9903398v3>

This figure "Fig3d.JPG" is available in "JPG" format from:

<http://arxiv.org/ps/cond-mat/9903398v3>

This figure "Fig4.JPG" is available in "JPG" format from:

<http://arxiv.org/ps/cond-mat/9903398v3>

This figure "Fig5.JPG" is available in "JPG" format from:

<http://arxiv.org/ps/cond-mat/9903398v3>

This figure "Fig6a.JPG" is available in "JPG" format from:

<http://arxiv.org/ps/cond-mat/9903398v3>

This figure "Fig6b.JPG" is available in "JPG" format from:

<http://arxiv.org/ps/cond-mat/9903398v3>

This figure "Fig7.JPG" is available in "JPG" format from:

<http://arxiv.org/ps/cond-mat/9903398v3>